Supporting information

Rational molecular design of electrolyte additive endows stable cycling performance of cobalt-free 5 V-class lithium metal batteries

*Wen-hui Hou[1,#], Yu Ou[1,#], Tianyou Zeng[2], Qingqing Feng[2], Pan Zhou[1], Yingchun Xia[2], Qingbin Cao[1], Weili Zhang[2], Xuan Song[1], Yang Lu[1], Shuaishuai Yan[1], Hangyu Zhou[3], Haiyu Zhou[1], Hao Liu[2], Fengxiang Liu[1] and Kai Liu[1]**

1. Department of Chemical Engineering, Tsinghua University, Beijing 100084, China
2. Tsinghua University Hefei Institute for Public Safety Research, Anhui 230601, China
3. China Academy of Safety Science and Technology, Beijing, 100012, China

* Corresponding author. E-mail: liukai2019@tsinghua.edu.cn

1. Experimental section

1.1. Synthesis of FS

72.4 mmol of 2-bromo-1,1-difluoroethane was added to an aqueous solution containing 68.9 mmol sodium thiomethoxide. The mixture was heated at 65°C for 10 hours to obtain 1,1-difluoro-2-(methylthio)ethane. After the methanol solution containing 89.2 mmol of 1,1-difluoro-2-(methylthio)ethane was cooled to 10 ℃, tantalum chloride and H_2O_2 solution was added into it. The mixture was heated to room temperature and maintained reaction at 45 °C for 3.5 hours. Then the mixture solution was concentrated under vacuum. The solid product was dissolved in 15 mL of dichloromethane, 8.1 g sodium sulfite was added and stirred for 30 minutes before filtration. The solid is dissolved in 15mL hexane, cooled in a refrigerator and filtered to obtain a precipitate. The precipitate was further filtered after recrystallization with 1:1 diether-hexane and dried under vacuum to obtain 2, 2-difluoroethyl methyl sulfone.

1.2. Materials

Battery-grade lithium salts (i.e., $LiPF_6$, LiDFOB) and organic solvents (FEC, EMC) were purchased from Duoduo chemical reagent Co., Ltd. 2032-type coin cells with Celegard 2325/25 μm separator were provided by Guangdong Canrd New Energy.

Metallic Li was purchased from China Energy Lithium. For the home-made LNMO cathode sheets, they were prepared by mixing LNMO particles, super-P and PVDF with a mass ratio of 90:5:5, and dried under vacuum overnight. The prepared electrodes were punched into 12 mm disks and the active material loading was about 7 mg cm^{-2} and 20 mg cm^{-2}.

1.3. Preparation of Electrolytes

The BEE electrolyte was composed of 1.0 M $LiPF_6$+0.2 M LiDFOB in FEC/EMC (1:3 by volume). The FSE electrolyte was prepared by adding 0.1 M FS into BEE electrolyte. All electrolytes were prepared in argon-filled glovebox (O_2<0.1 ppm, H_2O<0.1 ppm) at room temperature. The amount of electrolyte was controlled at 65 μL in all coin cells.

1.4. Electrochemical Measurements of coin-cell

All the electrochemical performance tests were performed based on 2032-type coin-cell assembled with 25 μm Celgard 2325 separator in argon-filled glove box. The LSV measurements of Li||stainless steel coin cells with different electrolytes were examined from open-circuit potential (OCP) to 5.5 V vs. Li at a scanning rate of 5 mV s^{-1}. The cyclic voltammetry (CV) measurements of Li|LNMO cells were examined between 3 and 4.9 V at a scanning rate of 1 mV s^{-1} under 25 °C. The residual BEE and FSE electrolytes after 15 CV cycles at 3-4.9 V was extracted for liquid chromatography-mass spectrometry (LC-MS) analysis. The leakage current test was performed in Li|LNMO cells with different electrolyte. The cells were first charged to 4.9 V and then maintained for 10000 s with the current monitored by Princeton electrochemical workstation. The Li|LNMO full cells were assembled with 40 μm thickness Li metals as anode and ~ 7 mg cm^{-2} LNMO sheets as cathode, then cycled at 1 C after two cycles at 0.1 C in the range of 3-4.9 V. For Li||Cu cells, Li foils with a diameter of 14 mm were used. The corresponding electrochemical impedance spectroscopy (EIS) after certain cycles was estimated at a frequency ranging from 0.1 HZ to 100000 HZ and fitted by Zview. The Tafel plots of symmetric Li|Li cells in different electrolytes was tested by Princeton electrochemical workstation.

1.5. Li |LNMO pouch cell assembly and electrochemical test

The pouch-type full cells were used to evaluate the practical application value of FSE electrolyte. The LNMO cathode with an active material mass ratio of 94% and areal mass loading of 32 mg cm^{-2} was provided by the 712th Research Institute of China Shipbuilding Industry Corporation. The dimensions of LNMO cathode and Li anode are 40 mm*70 mm and 50 mm*80 mm, respectively. 25 μm Celgard 2325 separator was employed. The amount of electrolyte added into the pouch cell was 3 g Ah^{-1}. The galvanostatic tests were performed within the voltage range of 3-4.9 V at 0.1C charge-discharge.

1.6. Material characterizations

Nuclear magnetic resonance (NMR) spectra were tested by Bruker Avance III HD 400 at room temperature. A scanning electron microscope (SEM, JSM-7200F) was conducted to characterize the surface morphology of electrodes. The X-ray diffraction (XRD) measurements of the samples were carried out on a Rigaku MiniFlex600. The LNMO cathode used for XPS and TOF-SIMS testing was obtained after 50 cycles at 0.5 C charge/discharge followed by cleaning with diethyl carbonate (DEC) solvent to remove the residual lithium salts. X-ray photoelectron spectrometer (XPS) spectra were obtained by Thermo Fisher Scientific ESCALAB Xi^{+}, with a sputtering rate of 30 nm/min (calibrated by SiO_2 /Si) in an area of 1 mm × 1 mm. The CEI components distribution was obtained by TOF-SIMS 5-100 (ION-TOF GmbH) operated at 30 keV using Bi^{3+} ion as probes and Cs^{+} accelerated at 1 keV. The analyzing area was 100 μm × 100 μm and the sputtering rate was controlled at 0.131 nm/s for SO_2. In situ surface-enhanced Raman spectroscopy (SERS) was performed in a sealed three-electrode electrochemical cell. A layer of coarse Au nanoparticles with a thickness of 20 nm was evaporated on the aluminum mesh as Raman enhanced working electrode. Lithium was applied as the reference electrode. The Raman scanning was carried out at different potentials (OCP vs Li, 3.4 V, 3.7 V, 4.0 V, 4.3 V) with a 532 nm diode laser.

EC-QCM instrument (Q-sense E4 system, Biolin Scientific, Sweden) was used to simultaneously measure the changes of both resonance frequency (Δf) and dissipation (ΔD) for the adsorption of electrolyte molecules on the quartz crystal sensor deposited with 2 nm Ni oxide layer. The EC-QCM applied a three-electrode configuration in

which the Pt plate serves as the counter electrode, the Ag/AgCl electrode serves as the reference electrode, and Au chip sputtered with Ni oxide layer as the working electrode. We in-situ replaced the electrolyte in the electrochemical chamber with BEE electrolyte or FSE electrolyte. The decrease in frequency and increase in dissipation caused by the adsorption of electrolyte components were recorded. In this work, the dissipation is small enough ($\Delta D<10\Delta f$), implying the adsorbed species form a rigid film with low viscoelasticity, so the Sauerbrey relation can be used to calculate the absorbed mass changes (Δm) based on the frequency changes:

$$\Delta m = -C * \frac{\Delta f}{n} \#$$

Where, the C is a constant characteristic of 17.7 $ng \cdot cm^{-2} \cdot Hz^{-1}$ for the quartz crystal, n is the overtone of the oscillations and n=3.

1.7. Theoretical calculation

The structures of lithium salts and solvents were fully optimized at the B3LYP-D3BJ/def2-SVP level of theory via the Gaussian 16 suite of programs. The solvent effect was included in the calculations using the solvation model based on the density (SMD) model. The vibrational frequencies of the optimized structures were carried out at the same level. The structures were characterized as a local energy minimum on the potential energy surface by verifying that all the vibrational frequencies were real. The molecular orbital levels of studied compounds were investigated via theoretical calculations, including the highest occupied molecular orbital (HOMO) and the lowest unoccupied molecular orbital (LUMO).

The adsorption energy and COHP calculations are performed in the framework of the density functional theory with the projector augmented plane-wave method, as implemented in the Vienna ab initio simulation package. The generalized gradient approximation proposed by Perdew, Burke, and Ernzerhof is selected for the exchange-correlation potential. The long-range van der Waals interaction is described by the DFT-D3 approach. The cut-off energy for plane wave is set to 500 eV. The electronic energy was considered self-consistent when the energy change was smaller than 10^{-5} eV. A geometry optimization was considered convergent when the energy change was

smaller than 0.02 eV $Å^{-1}$. In our structure, the U correction is used for Ni and Mn atoms. The vacuum spacing in a direction perpendicular to the plane of the structure is 15 Å for the surfaces. The Brillouin zone integration is performed using 3×2×1 Monkhorst-Pack k-point sampling for a structure. Finally, the adsorption energies (E_{ads}) were calculated as $E_{ads}= E_{total} -E_{mol} -E_{sub}$, where E_{total}, E_{mol}, and E_{sub} are the total energies of the optimized adsorbate/substrate system, the adsorbate in the structure, and the clean substrate, respectively. The projected crystal orbital Hamiliton population (pCOHP) was obtained by LOBSTER program.

2. Supporting Figures and tables

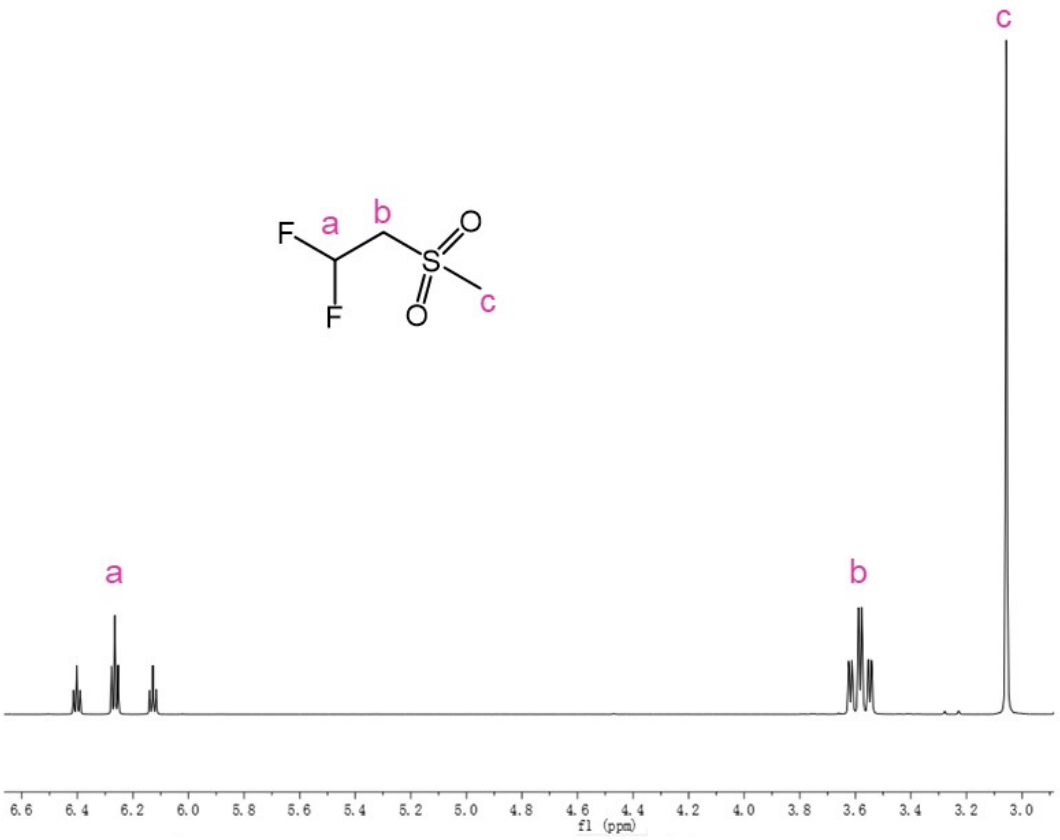

Figure S1. ^{1}H NMR spectrum of FS in $CDCl_3$.

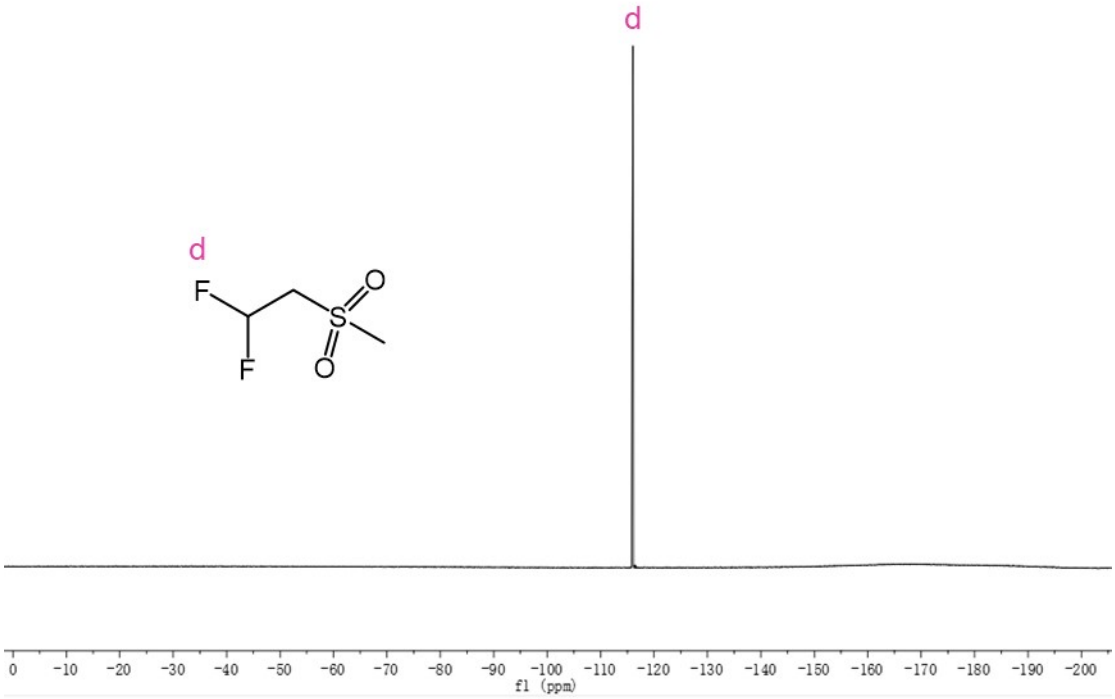

Figure S2. ^{19}F NMR spectrum of FS in $CDCl_3$.

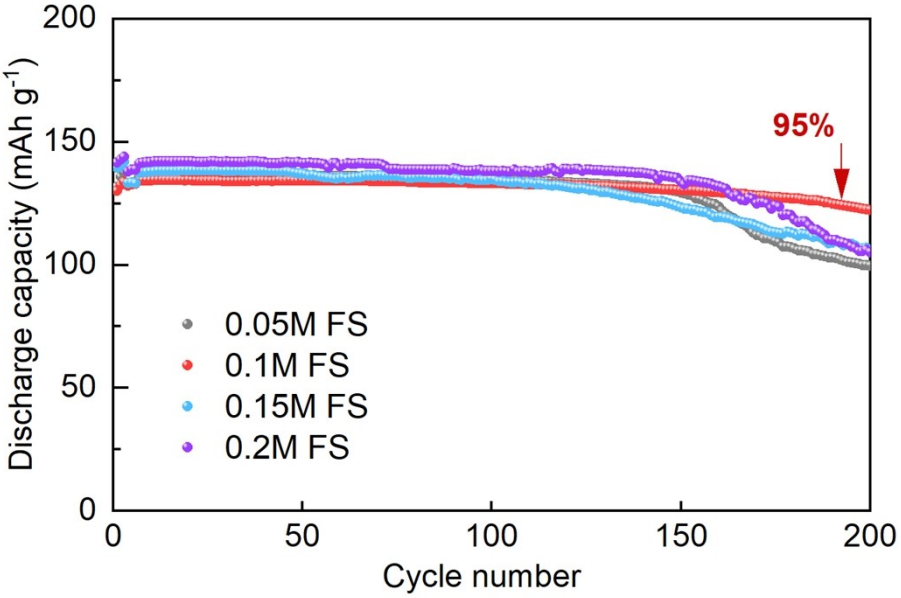

Figure S3. The concentration optimization test of FS on the basis of Li/LNMO cells with cathode loading of 10 mg cm^{-2} at 0.5 C between 3-4.9 V.

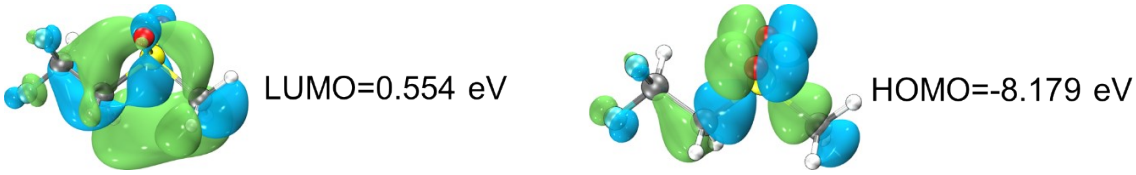

Figure S4. The LUMO and HOMO energy levels of FS.

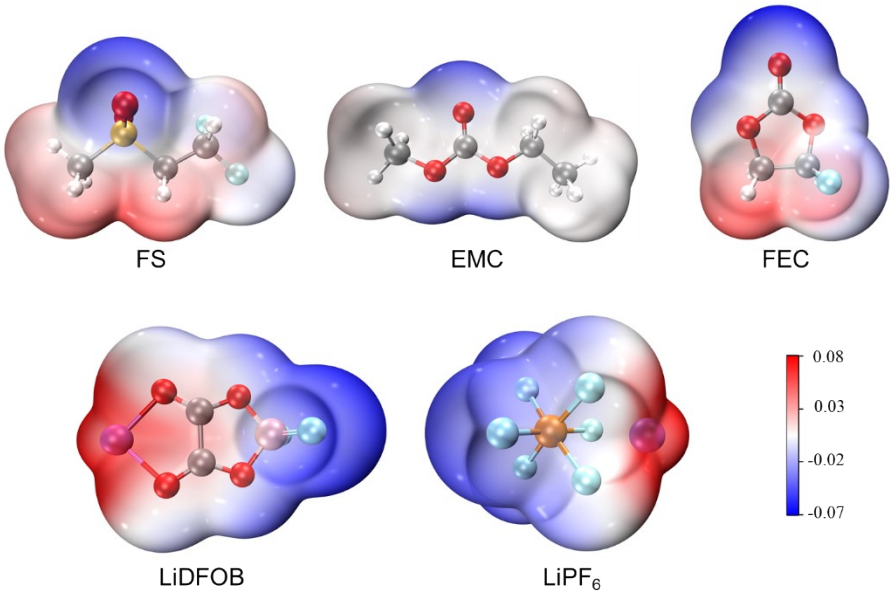

Figure S5. Calculated electrostatic potential maps of each component in electrolytes under vacuum conditions.

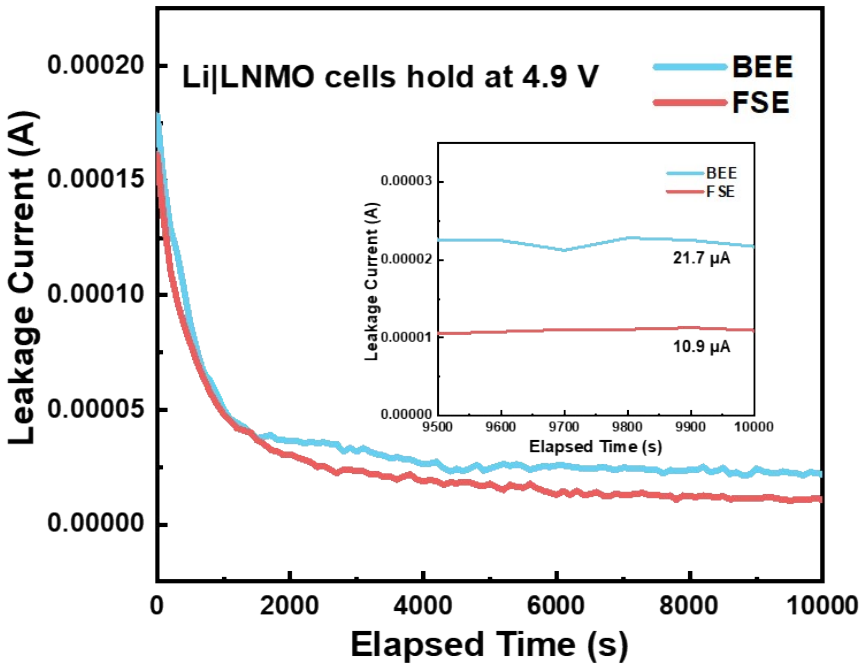

Figure S6. Leakage currents of Li|LNMO cells using BEE and FSE electrolytes at a constant applied voltage of 4.9 V and a temperature of 25 °C.

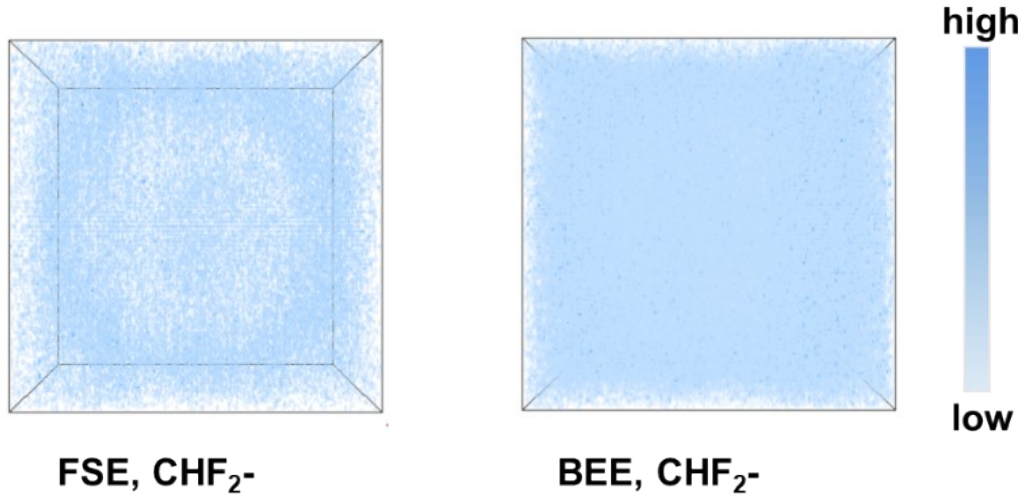

Figure S7. The distribution of the CHF_2- species in the TOF-SIMS sputtered surface of the cycled LNMO in FSE and BEE electrolytes.

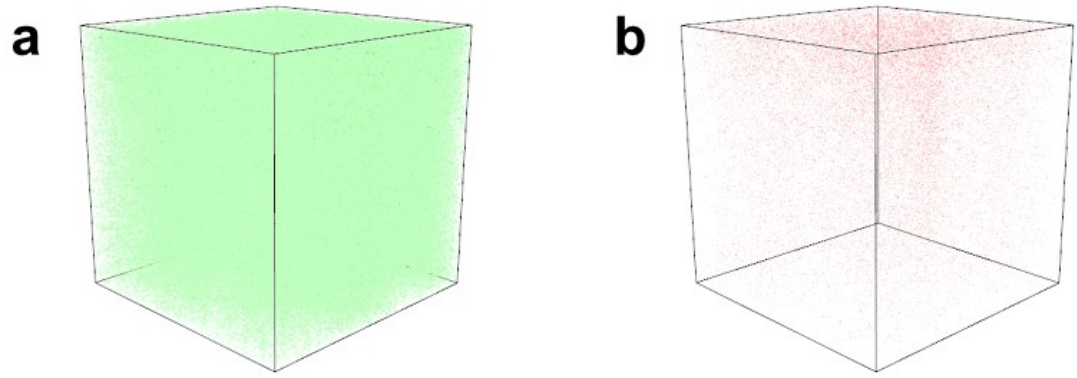

Figure S8. The distribution of the S- species (a) and SO_2- (b) in the TOF-SIMS sputtered surface of the cycled LNMO in FSE electrolytes.

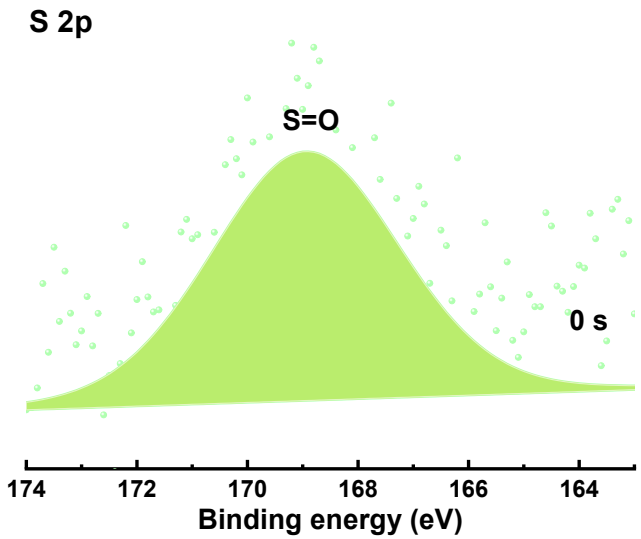

Figure S9. S 2p XPS spectrum of the cycled LNMO in FSE electrolyte at 0 s sputtering time.

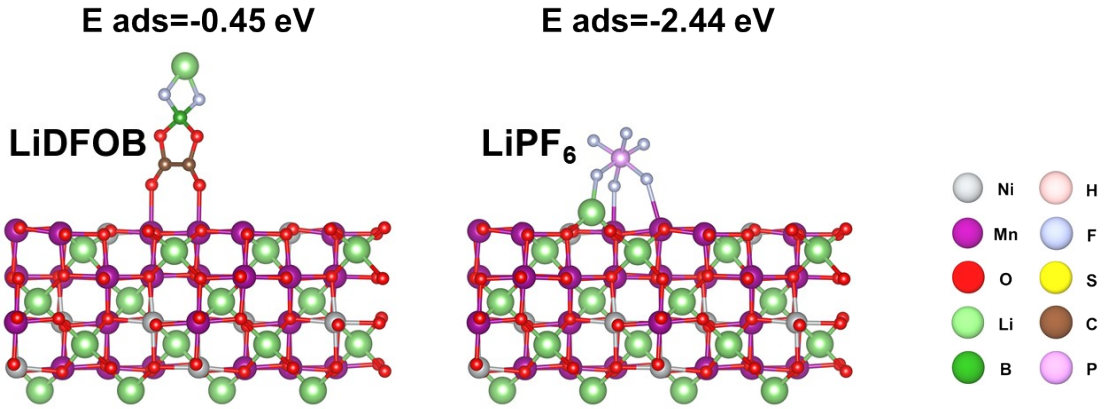

Figure S10. Adsorption energies of LiDFOB and $LiPF_6$ on the (001) plane of $LiNi_{0.5}Mn_{1.5}O_4$.

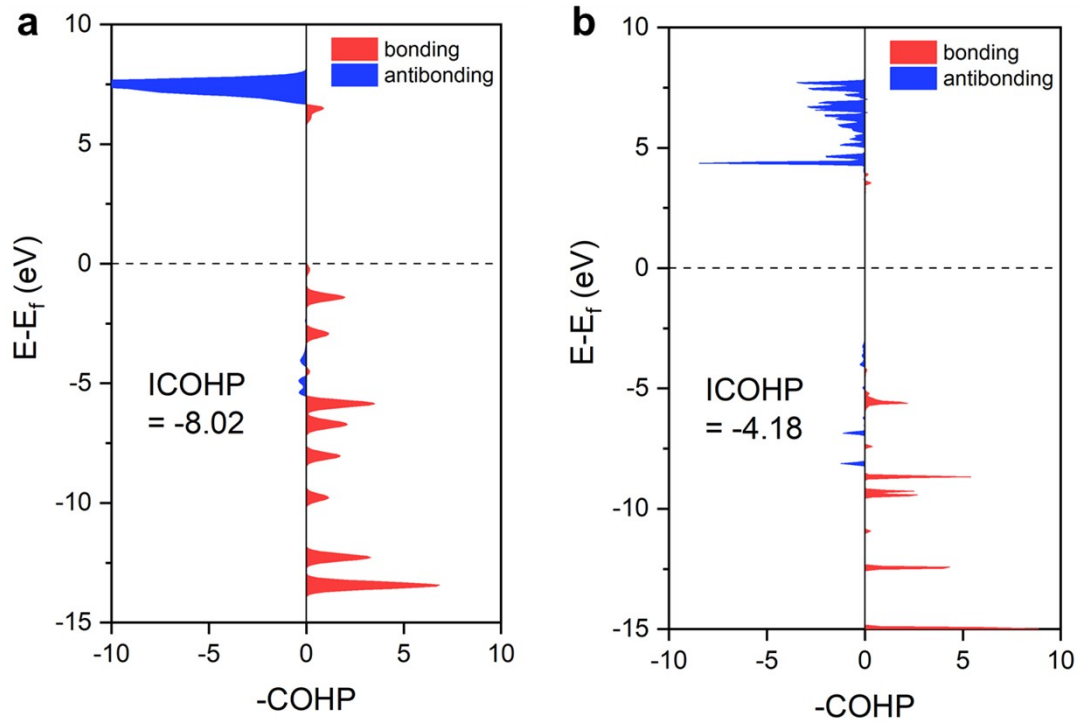

Figure S11. The crystal orbital overlapping population of the C-C bond analysis for $–CH_2-CHF_2$ before (a) and after adsorption, in which the Fermi energy is set to 0 eV. The crystal orbital Hamilton population is abbreviated as COHP.

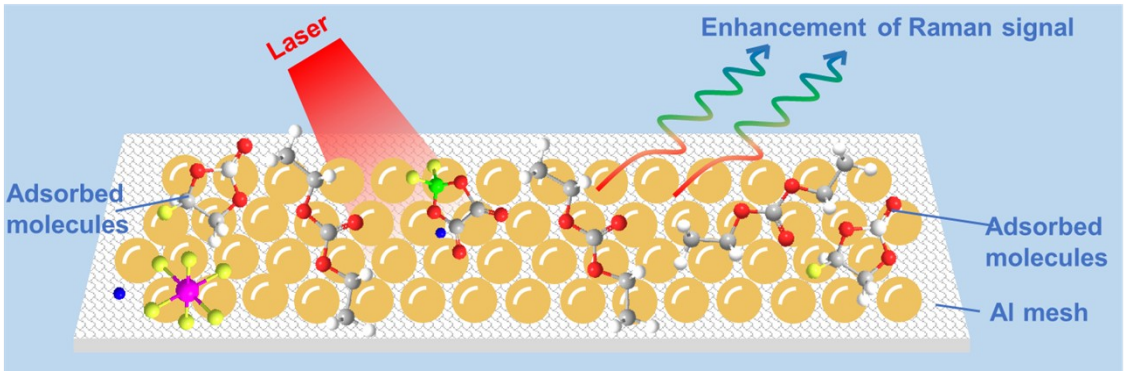

Figure S12. Schematic of an in situ EC-SERS cell, which was composed of a gold-sprayed Al mesh as a working electrode, a lithium foil as a reference electrode and counter electrode.

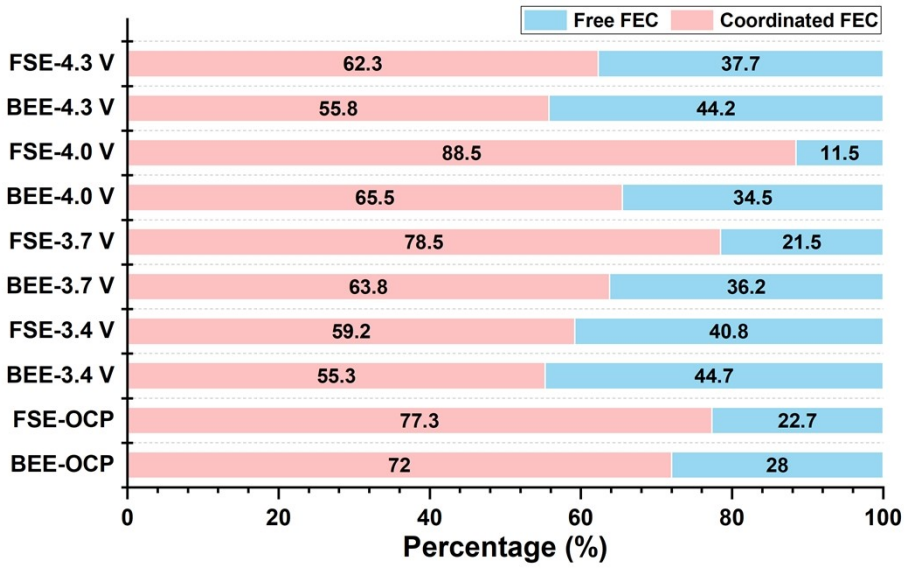

Figure S13. The percentage of free FEC and coordinated FEC in FSE and BEE electrolytes under different external potential.

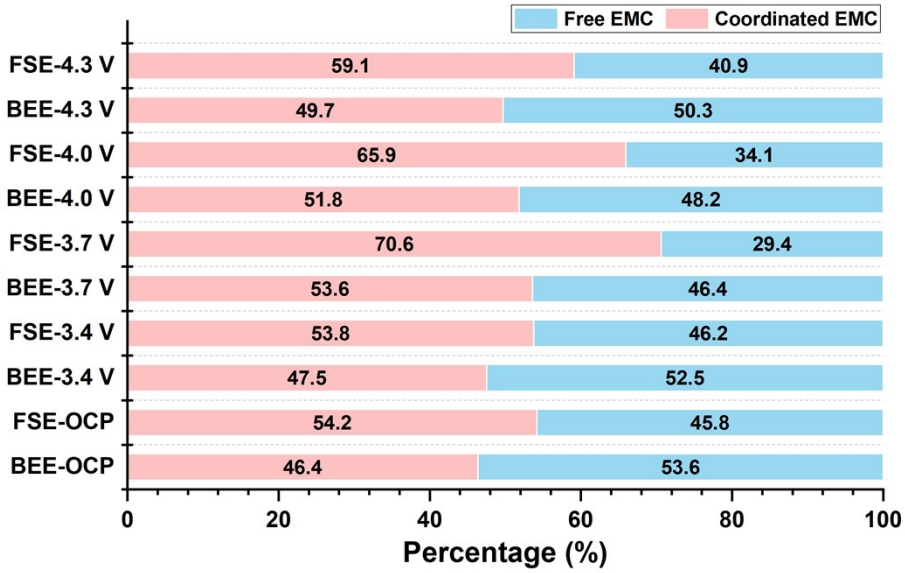

Figure S14. The percentage of free EMC and coordinated EMC in FSE and BEE electrolytes under different external potential.

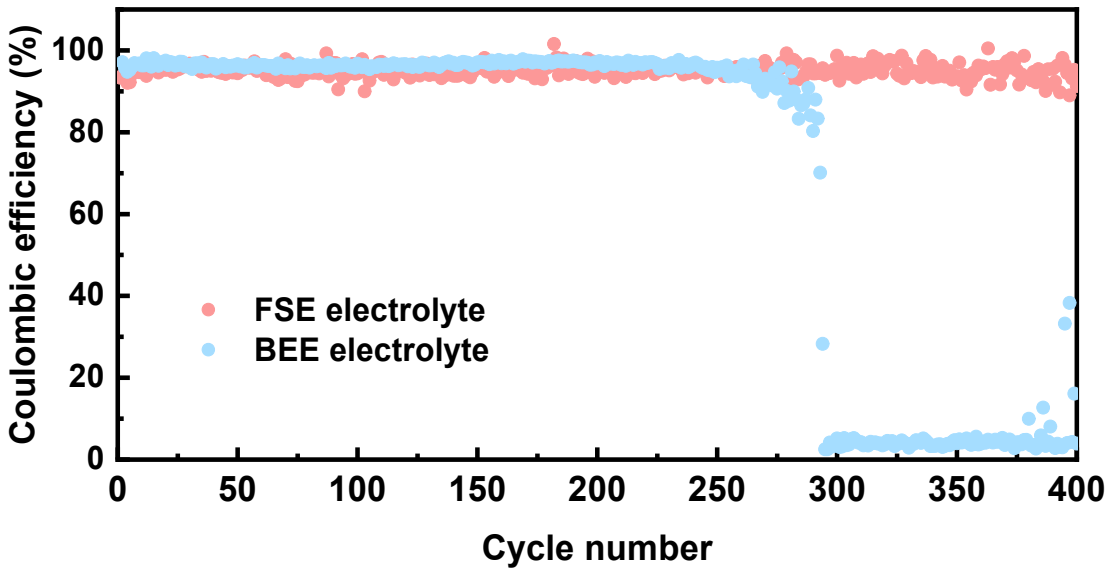

Figure S15. Li-Cu cells galvanostatic cycling with a capacity of 1 mAh cm^{-2} at a 1 mA cm^{-2}.

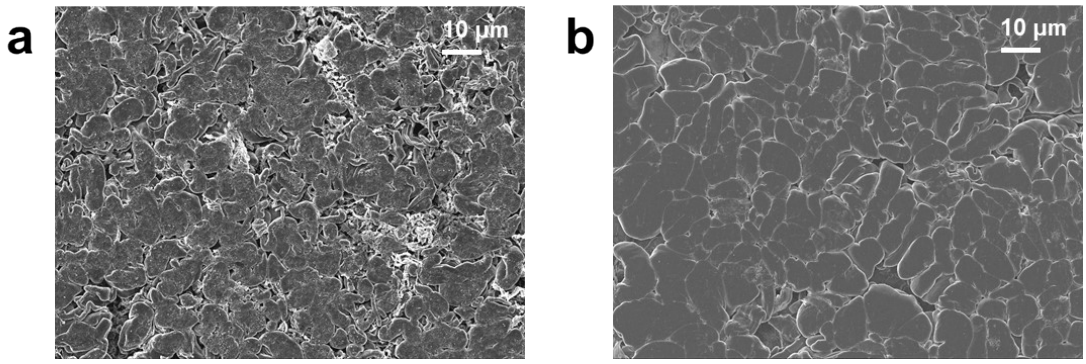

Figure S16. SEM images of the LMAs after 2 cycles at 1.0 mA cm^{-2} and 1.0 mAh cm^{-2} in BEE electrolyte (a) and FSE electrolyte (b).

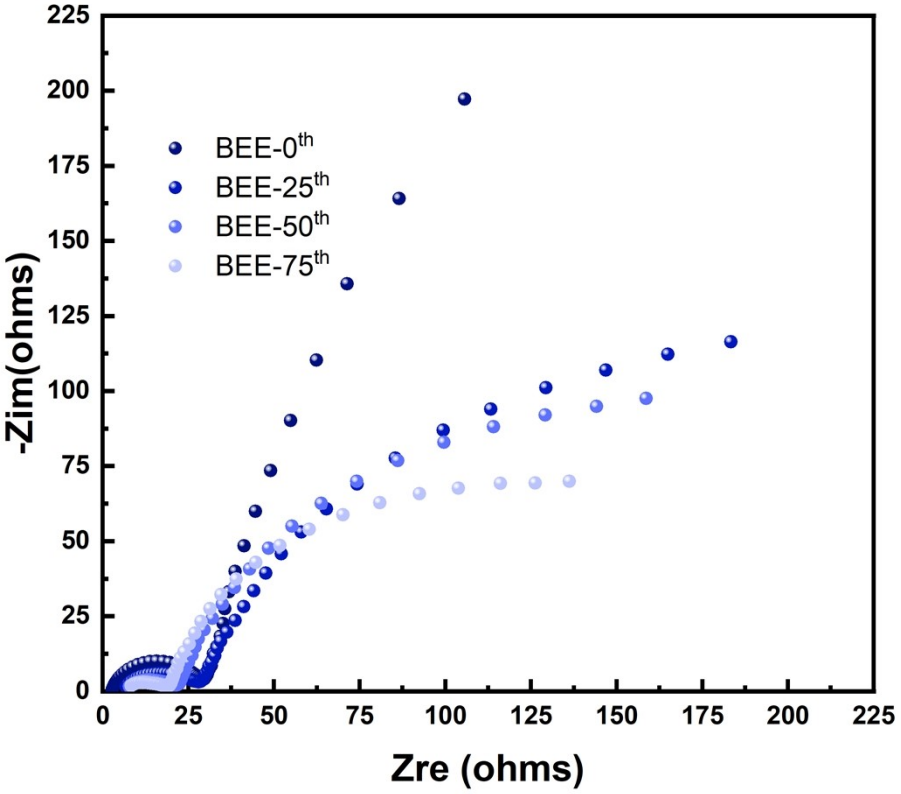

Figure S17. Nyquist plots of Li|Cu cells after different cycles in BEE electrolyte.

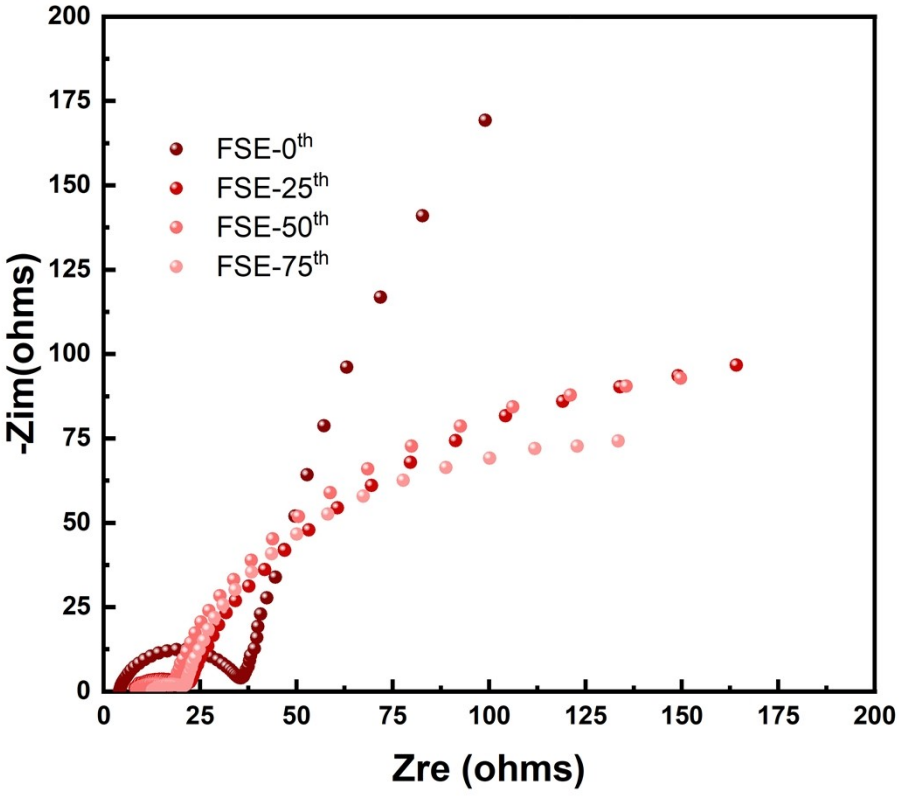

Figure S18. Nyquist plots of Li|Cu cells after different cycles in FSE electrolyte.

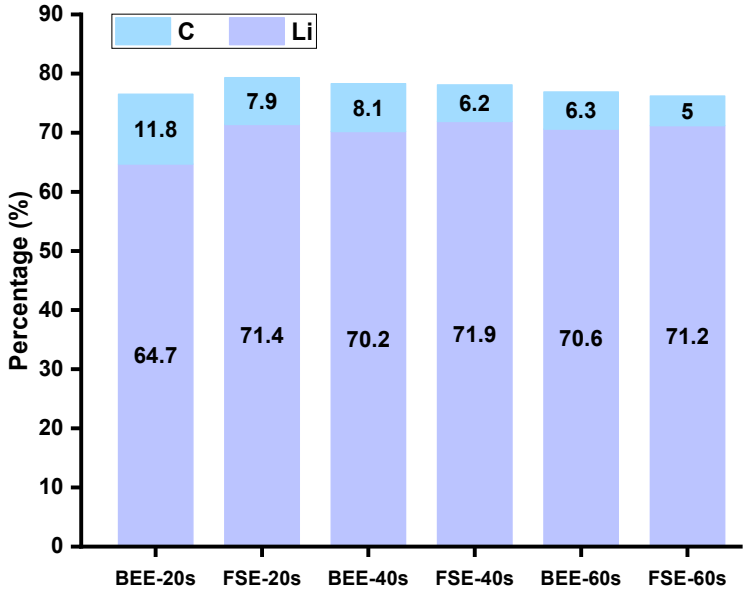

Figure S19. The atomic ratio of C 1s and Li 1s at different etching depth of the cycled LMAs with BEE electrolyte or FSE electrolyte.

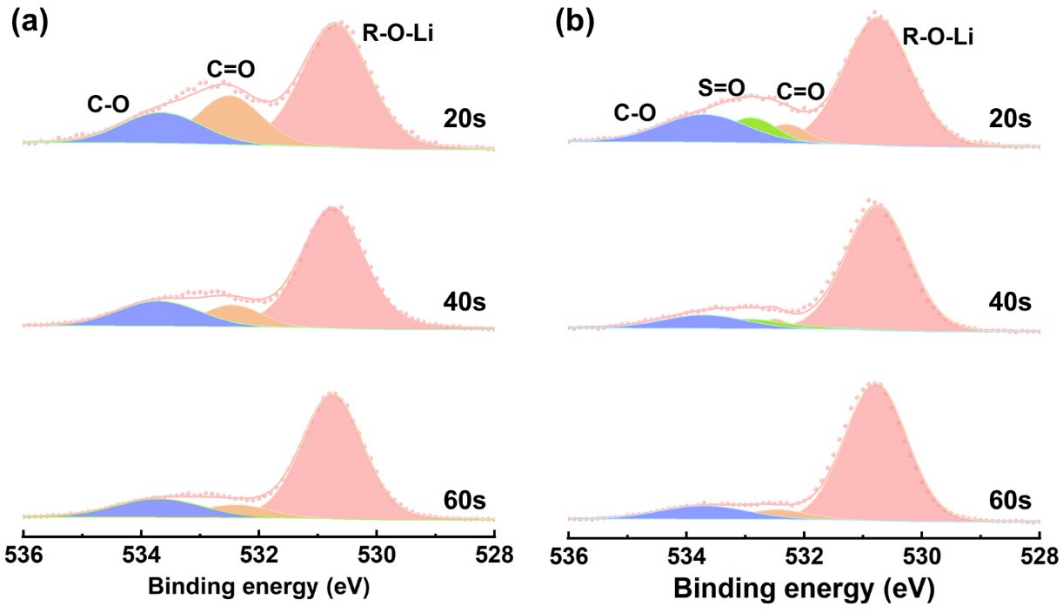

Figure S20. O 1s XPS spectra of the cycled LMAs in BEE electrolyte (a) and FSE electrolyte (b).

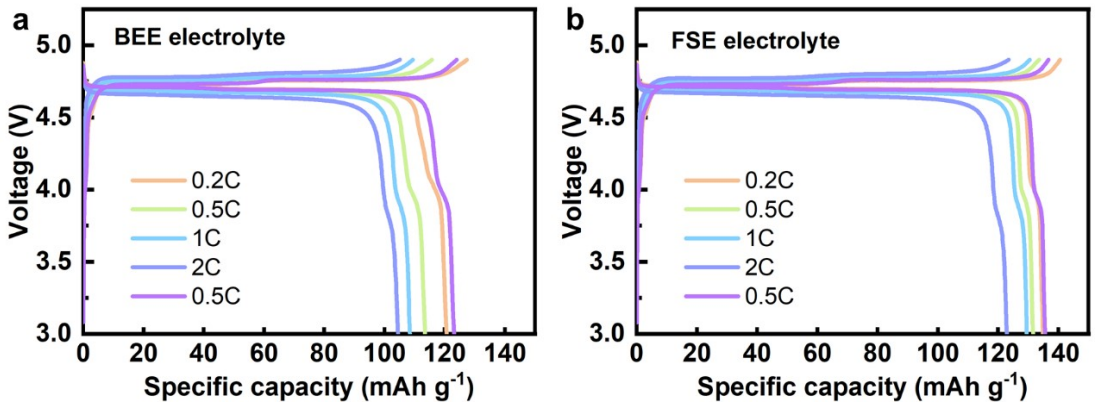

Figure S21. Voltage curves of BEE electrolyte (a) and FSE electrolyte (b) under different current rates from 0.2 C to 2 C.

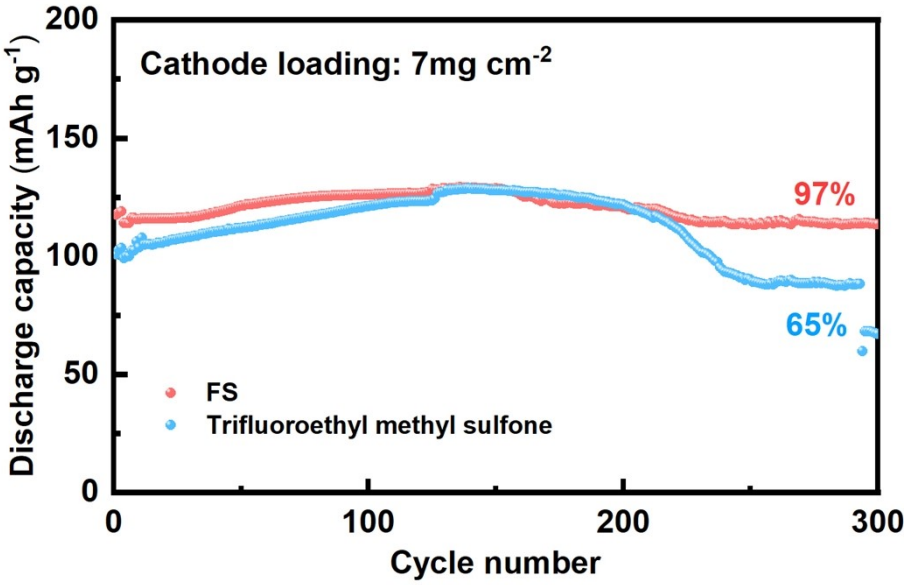

Figure S22. Long-term cycling performances of Li/LNMO half cells at 0.5 C between 3-4.9 V.

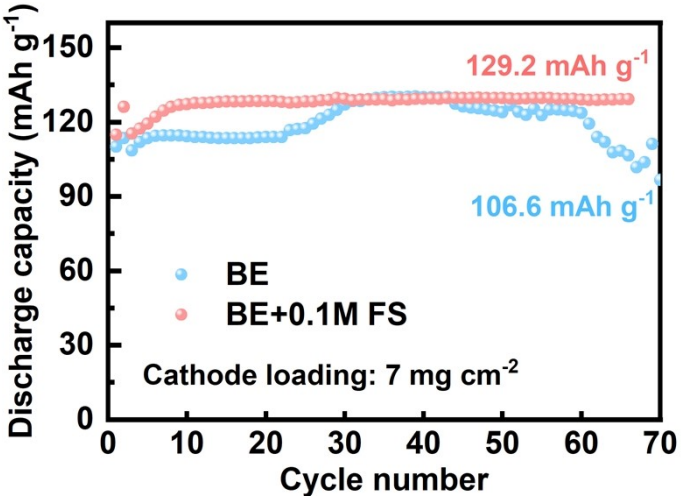

Figure S23. Long-term cycling performances of Li/LNMO half cells at 0.5 C between 3-4.9 V based on the 1M $LiPF_6$ in EC/DMC (v/v=1/1) (abbreviated as BE).

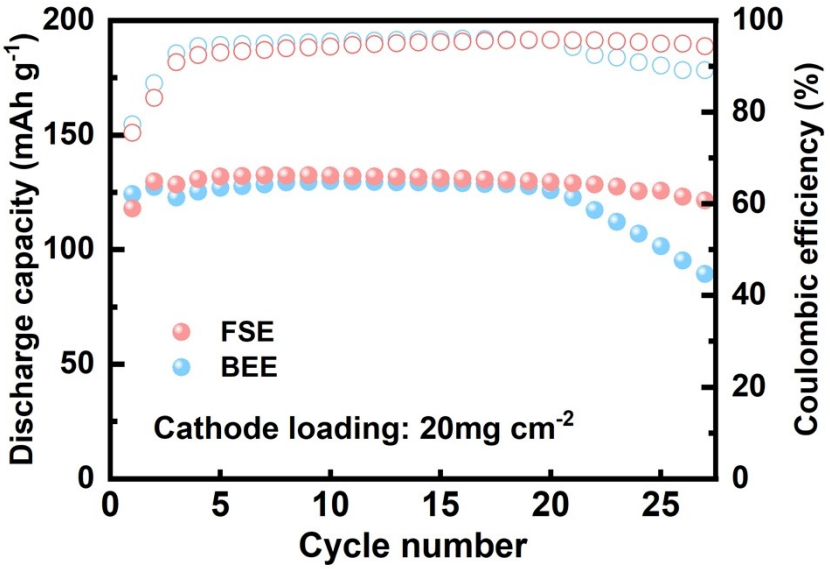

Figure S24. Cycling performances of Li/LNMO half cells with cathode loading of 20 mg cm^{-2} between 3-4.9 V under 60°C.

Table S1. Ionic conductivity of BEE and FSE electrolytes tested with a Celgard 2325 separator.

Electrolyte	Conductivity (mS/cm^2)
BEE electrolyte	0.41
FSE electrolyte	0.42

Table S2. Comparison of our work with recent electrolyte works on LNMO-based lithium metal batteries.

Electrolyte	Cathode	Anode	Batter type	Cell voltage	Capacity retention
1M $LiPF_6$ in FEC/EMC (v/v=1/3)+0.2M LiDFOB+0.1M FS (This work)	**LNMO 7 mg cm^{-2}**	**Li metal 40 um**	**Full cell**	**3-4.9 V, 1 C**	**600 cycles, 84%; 500 cycles, 88%; 400 cycles, 92%; 300 cycles, 95%; 200 cycles, 97%**
	LNMO 20 mg cm^{-2}	**Li metal 40 um**	**Full cell**	**3-4.9 V, 1 C**	**100 cycles, 99%**
1M $LiPF_6$ in EC DEC+0.5%NFSA **(ref.[1])**	LNMO 3 mg cm^{-2}	Li metal, thickness not mentioned	Half cell	3-5 V, 1 C	400 cycles, 93%
1M $LiPF_6$ in DMDOHD **(ref.[2])**	LNMO 10 mg cm^{-2}	Li metal, thickness not mentioned	Half cell	3.5-4.9 V, 0.2 C	200 cycles, 94%
1M $LiPF_6$ in EC/DEC (v/v=1/1) +10% PFPN **(ref.[3])**	LNMO 11 mg cm^{-2}	Li metal 50 um	Full cell	3-4.9 V, 0.5 C	100 cycles, 90.7%
1.2M $LiPF_6$ in EC/DMC(v/v=3/7)+0.1wt% MPS **(ref.[4])**	LNMO 2.5 mg cm^{-2}	Li metal, thickness not mentioned	Half cell	3.5-4.9 V, 1 C	400 cycles, 89.3%
1M $LiPF_6$ in EC/DEC (v/v=1/1)+0.2wt% PFPDPP **(ref.[5])**	LNMO 1 mg cm^{-2}	Li metal, thickness not mentioned	Half cell	3-5 V, 2 C	300 cycles, 71%
1M $LiPF_6$ in EC/DMC/EMC (v/v/v=111)+0.1wt% DPE **(ref.[6])**	LNMO 3 mg cm^{-2}	Li metal, thickness not	Half cell	3.5-4.95 V, 1 C	100 cycles, 90.5%

		mentioned			
1.15M $LiPF_6$ EC/DEC (v/v=1/1) + 1 wt% DMAc + 10 wt.% TEMEP-TFSI **(ref.[7])**	LNMO 7 mg cm^{-2}	Li metal, thickness not mentioned	Half cell	3-4.9 V, 0.5 C	100 cycles, 92.6%
1M $LiPF_6$ in EC/EMC/DEC (v/v/v=3/5/2) +0.3% MPL **(ref.[8])**	LNMO 1.6 mg cm^{-2}	Li metal, thickness not mentioned	Half cell	3.5-5 V, 0.5 C	200 cycles, 89.5%
1M $LiPF_6$ in EC/EMC/DEC (v/v/v=3/5/2) +0.25% SE **(ref.[9])**	LNMO 3.1 mg cm^{-2}	Li metal, thickness not mentioned	Half cell	3-4.9 V, 1 C	100 cycles, 88%
1M $LiPF_6$ in EC/DMC (v/v =1/3) +1M FEC+25Mm HDI **(ref.[10])**	LNMO 1 mg cm^{-2}	Li metal, thickness not mentioned	Half cell	3.5-4.9 V, 0.5 C	200 cycles, 76.1%

References

1 J. Zhou, B. Hao, M. Peng, L. Zhang, H. Ji, J. Liu, W. Ling, C. Yan and T. Qian, *Adv. Energy Mater.*, 2023, **13**.

2 X. Zhang, P. Xu, J. Duan, X. Lin, J. Sun, W. Shi, H. Xu, W. Dou, Q. Zheng, R. Yuan, J. Wang, Y. Zhang, S. Yu, Z. Chen, M. Zheng, J.-F. Gohy, Q. Dong and A. Vlad, *Nat. Commun.*, 2024, **15**, 536.

3 Q. Liu, Z. Chen, Y. Liu, Y. Hong, W. Wang, J. Wang, B. Zhao, Y. Xu, J. Wang, X. Fan, L. Li and H. B. Wu, *Energy Stor. Mater.*, 2021, **37**, 521-529.

4 Y. Huang, Y. Li, C. Tan, Z. Huang, Q. Pan, Y. Chu, F. Zheng, H. Wang and Q. Li, *ACS Appl. Energy Mater.*, 2021, **5**, 639-647.

5 S. Bolloju, C.-Y. Chiou, T. Vikramaditya and J.-T. Lee, *Electrochim. Acta*, 2019, **299**, 663-671.

6 S.-Y. Bae, W.-K. Shin and D.-W. Kim, *Electrochim. Acta*, 2014, **125**, 497-502.

7 H. Y. Yue, Z. L. Han, L. L. Tao, Y. F. Zhang, L. Wang, X. N. Li, Y. H. Yin, W. G. Yang and S. T. Yang, *ChemElectroChem.*, 2018, **5**, 1509-1515.

8 J. Chen, Y. Gao, C. Li, H. Zhang, J. Liu and Q. Zhang, *Electrochim. Acta*, 2015, **178**, 127-133.

9 W. Tu, C. Ye, X. Yang, L. Xing, Y. Liao, X. Liu and W. Li, *J. Power Sources*, 2017, **364**, 23-32.

10 D. Sun, Q. Wang, J. Zhou, Y. Lyu, Y. Liu and B. Guo, J. Electrochem. Soc., 2018, **165**, A2032-A2036.